Title

Upper tropospheric ozone production from lightning NOx-impacted convection: Smoke ingestion case study from the DC3 campaign

Journal

Journal of Geophysical Research, 120(6)

ISSN

0148-0227

Authors

Apel, EC
Hornbrook, RS
Hills, AJ
et al.

Publication Date

2015

DOI

10.1002/2014JD022121

AGU PUBLICATIONS

JGR

Journal of Geophysical Research: Atmospheres

RESEARCH ARTICLE
10.1002/2014JD022121

Special Section:
Deep Convective Clouds and Chemistry 2012 Studies (DC3)

Key Points:
- Lightning NO_x is a key driver of ozone production in storm outflows
- Storms can transport biomass burning emissions to the upper troposphere
- Acrolein is shown to be a good tracer for fresh biomass burning emissions

Correspondence to:
E. C. Apel,
apel@ucar.edu

Citation:
Apel, E. C., et al. (2015), Upper tropospheric ozone production from lightning NO_x-impacted convection: Smoke ingestion case study from the DC3 campaign, *J. Geophys. Res. Atmos.*, *120*, 2505–2523, doi:10.1002/2014JD022121.

Received 2 JUN 2014
Accepted 31 JAN 2015
Accepted article online 6 FEB 2015
Published online 21 MAR 2015

Upper tropospheric ozone production from lightning NO_x-impacted convection: Smoke ingestion case study from the DC3 campaign

E. C. Apel[1], R. S. Hornbrook[1], A. J. Hills[1], N. J. Blake[2], M. C. Barth[1], A. Weinheimer[1], C. Cantrell[3], S. A. Rutledge[4], B. Basarab[4], J. Crawford[5], G. Diskin[5], C. R. Homeyer[1], T. Campos[1], F. Flocke[1], A. Fried[3], D. R. Blake[2], W. Brune[6], I. Pollack[7], J. Peischl[7], T. Ryerson[7], P. O. Wennberg[8], J. D. Crounse[8], A. Wisthaler[9,10], T. Mikoviny[9,10], G. Huey[11], B. Heikes[12], D. O'Sullivan[13], and D. D. Riemer[14]

[1]Atmospheric Chemistry Division, National Center for Atmospheric Research, Boulder, Colorado, USA, [2]School of Physical Sciences, University of California, Irvine, California, USA, [3]Department of Atmospheric and Oceanic Sciences, University of Colorado Boulder, Boulder, Colorado, USA, [4]Department of Atmospheric Science, Colorado State University, Fort Collins, Colorado, USA, [5]NASA Langley Research Center, Hampton, Virginia, USA, [6]Department of Meteorology, Pennsylvania State University, University Park, Pennsylvania, USA, [7]Chemical Sciences Division, Earth System Research Laboratory, National Oceanic and Atmospheric Administration, Boulder, Colorado, USA, [8]Division of Geological and Planetary Sciences, California Institute of Technology, Pasadena, California, USA, [9]Department of Chemistry, University of Oslo, Oslo, Norway, [10]Institute of Ion Physics and Applied Physics, University of Innsbruck, Innsbruck, Austria, [11]School of Earth and Atmospheric Sciences, Georgia Institute of Technology, Atlanta, Georgia, USA, [12]Graduate School of Oceanography, University of Rhode Island, Kingston, Rhode Island, USA, [13]Chemistry Department, United States Naval Academy, Annapolis, Maryland, USA, [14]Rosenstiel School of Marine and Atmospheric Science, University of Miami, Coral Gables, Florida, USA

Abstract As part of the Deep Convective Cloud and Chemistry (DC3) experiment, the National Science Foundation/National Center for Atmospheric Research (NCAR) Gulfstream-V (GV) and NASA DC-8 research aircraft probed the chemical composition of the inflow and outflow of two convective storms (north storm, NS, south storm, SS) originating in the Colorado region on 22 June 2012, a time when the High Park wildfire was active in the area. A wide range of trace species were measured on board both aircraft including biomass burning (BB) tracers hydrogen cyanide (HCN) and acetonitrile (ACN). Acrolein, a much shorter lived tracer for BB, was also quantified on the GV. The data demonstrated that the NS had ingested fresh smoke from the High Park fire and as a consequence had a higher VOC OH reactivity than the SS. The SS lofted aged fire tracers along with other boundary layer ozone precursors and was more impacted by lightning NO_x (LNO_x) than the NS. The NCAR master mechanism box model was initialized with measurements made in the outflow of the two storms. The NS and SS were predicted to produce 11 and 14 ppbv of O_3, respectively, downwind of the storm over 2 days. Sensitivity tests revealed that the ozone production potential of the SS was highly dependent on LNO_x. Normalized excess mixing ratios, $\Delta X/\Delta CO$, for HCN and ACN were determined in both the fire plume and the storm outflow and found to be 7.0 ± 0.5 and 2.3 ± 0.5 pptv ppbv^{-1}, respectively, and 1.4 ± 0.3 pptv ppbv^{-1} for acrolein in the outflow only.

1. Introduction

Thunderstorms and pyroconvective storms can serve as conduits for redistributing both long- and short-lived HO_x and ozone precursors from the lower troposphere (LT) to the upper troposphere (UT) and even into the stratosphere [e.g., *Dickerson et al.*, 1987; *Dye et al.*, 2000; *Brunner et al.*, 1998; *Crawford et al.*, 2000; *Fromm et al.*, 2000; *Jost et al.*, 2004]. Species such as hydrogen peroxide (H_2O_2), methyl hydroperoxide (CH_3OOH) [*Snow et al.*, 2007], formaldehyde (CH_2O) [*Colomb et al.*, 2006; *Stickler et al.*, 2006; *Fried et al.*, 2008], isoprene, and isoprene oxidation products [*Apel et al.*, 2012] have been shown to be transported to the UT through this process. Lightning associated with storms produces substantial amounts of nitrogen oxides ($NO_x = NO + NO_2$) [e.g., *Ridley et al.*, 1994, 2004], and its influence in the UT is generally thought to be greater than currently represented in global models [*Singh et al.*, 2007; *Hudman et al.*, 2007] although a recent study presented an optimized regional scaling algorithm to fit lightening NO_x sources to satellite lightning data in a way that preserves the coupling to deep convective transport [*Murray et al.*, 2012] . The UT is a chemically important region of the atmosphere where small changes can have large effects; it is well known that ozone is an important greenhouse gas

[*Intergovernmental Panel on Climate Change*, 2013], and *Lacis et al*. [1990] and *Forster and Shine* [1997] showed that ozone increases near the tropopause raise surface temperatures more than similar increases in ozone elsewhere in the troposphere. Thus, it is important to obtain information on the redistribution of precursors from the LT to the UT and chemical processes that result from this that affect ozone chemistry in the UT region.

The impact of vertical transport on the photochemistry of the UT is ultimately dependent upon the boundary layer (BL) emissions of VOCs and NO_x and on lightning NO_x (LNO_x) occurring within the storms whose outflow reaches the UT. On a global scale, biogenic emissions account for the majority of the VOC emissions. However, for the Colorado Front Range in June the majority of BL emissions are from vehicles, agriculture, and the oil and gas industry [*Pétron et al*., 2012, 2014; *Gilman et al*., 2013]. NO_x sources are dominated by vehicle and power plant point emissions. Fires can add significant quantities of NO_x and VOCs including OVOCs, and these can have a large impact on the air quality in the region during summertime.

A goal of the Deep Convective Clouds and Chemistry (DC3) campaign (M. Barth et al., The deep convective clouds and chemistry campaign, *Bulletin of the American Meteorological Society*, unpublished, 2015), conducted between 10 May and 30 June 2012, with operations out of Salina, Kansas, was to investigate the impact of deep midlatitude convection on UT composition and chemistry with an understanding that lightning plays a large role in this; modeling studies [*Pickering et al*., 1990; *Apel et al*., 2012] have shown the importance of LNO_x in increasing the ozone-forming potential in the outflow of convected air masses. This paper presents a case study for determining the ozone-forming potential for the outflow from two storms, one that was more impacted by LNO_x than the other and one that was more impacted by fresh biomass burning (BB) emissions than the other. An overview of the methods used to characterize the presence and impact of lightning during this study is given by (M. Barth et al., unpublished, 2015).

One way to detect the transport of fire plumes into the UT is by quantifying HCN, which has proven to be valuable in air chemistry studies as a reliable tracer of BB emissions [e.g., *Singh et al*., 2003; *Yokelson et al*., 2007a, 2007b; *Crounse et al*., 2009]. Although it has a photochemical lifetime of approximately 4 years, the tropospheric residence lifetime of HCN is on the order of months because it is presumed to be deposited to the ocean surface [*Li et al*., 2000, 2003; *Singh et al*., 2003]; the relatively long lifetime in the free troposphere allows for this species to be distributed throughout the troposphere, and HCN has been observed in satellite imagery deep into the stratosphere as a consequence of BB entrained into the Asian monsoon circulation [*Randel et al*., 2010]. Acetonitrile (CH_3CN and ACN) is another species known to have significant emissions from fires. It is also quite unreactive and believed to be removed primarily through deposition to the ocean [*Hamm and Warneck*, 1990]; it is similarly distributed throughout the troposphere and has been used to track both local fire emissions [e.g., *Yokelson et al*., 2007a] and transocean and transcontinental advection of BB plumes [*Singh et al*., 2003; *de Gouw et al*., 2006; *Warneke et al*., 2009].

The primary atmospheric chemical sink for both HCN and ACN is from reaction with OH [*Singh et al*., 2003] resulting in photochemical lifetimes on the order of 4 years for HCN (as mentioned previously) and 2 years for ACN. Although BB is believed to be the primary source for both HCN [*Li et al*., 2000, 2003, 2009; *Shim et al*., 2007] and ACN [*Singh et al*., 2003; *de Gouw et al*., 2003] in the atmosphere, uncertainties remain in understanding the tropospheric budgets of these species in part because of an insufficient number of measurements, particularly for HCN since fewer techniques are available for its measurement. For ACN the database has increased substantially during the last decade as the result of the widespread deployment of mass spectrometric techniques (proton transfer reaction-mass spectrometry (PTR-MS) and the Trace Organic Gas Analyzer (TOGA)) that can easily measure it.

Acrolein (CH_2CHCHO) is a toxic, highly reactive unsaturated aldehyde that is produced by the incomplete combustion of organic material [*Lipari et al*., 1984] and vehicle exhaust as well as the oxidation of atmospheric chemical precursors such as 1,3-butadiene (a component of motor vehicle exhaust and fire emissions). However, a recent study conducted in a region strongly impacted by motor vehicles [*Spada et al*., 2008] showed that acrolein concentrations did not correlate with traffic density, ozone concentrations, or tracers of direct vehicle emissions, suggesting that BB is the predominant source and not vehicles either through primary emissions or secondary oxidation products. Two recent studies documented acrolein emissions in laboratory-controlled burning experiments [*Warneke et al*., 2011; *Kostenidou et al*., 2013] providing further evidence that acrolein may be a useful BB burning tracer. Although considered by regulatory agencies to be one of the most dangerous components of toxic air mixtures, acrolein is typically not reported in studies

ofcarbonyls in the atmosphere because its mixing ratio is often below the limit of detection of the instruments used in the studies. Because of its BB source, its high reactivity, and consequent short lifetime ($\approx$4 h at [OH] = 3.7×10^6 molecules cm^{-3}, average OH measured during the afternoon hours, approximately 1–5 P.M. local time), acrolein is a good candidate for use as a tracer of fresh fire emissions. However, detecting acrolein from aircraft in diluted fire plumes is challenging because mixing ratios of acrolein decrease rapidly with time. The technique described here has sufficient sampling frequency and sensitivity to be useful for ambient aircraft-based measurements. The details of this technique will be described in another paper (Apel et al., in preparation).

The extensively instrumented aircraft used in the study described here included the National Science Foundation (NSF)/National Center for Atmospheric Research (NCAR) Gulfstream-V (GV), the National Aeronautic and Space Administration (NASA) DC-8, and ground-based observations used to characterize storms from below and satellites from above in the DC3 domain (M. Barth et al., unpublished, 2015). The GV aircraft was the primary platform to study the high-altitude outflow of the storms. The GV also targeted the subsequent downwind chemical evolution following convection. The DC-8 aircraft worked closely with the GV and had a primary mission objective to characterize the convective storm inflow. Reversing roles, the GV occasionally measured inflow, and the DC-8 occasionally measured outflow, principally to obtain data for trace gases and aerosols that were not measured on the GV.

On 22 June both the DC-8 and the GV flew to Colorado to study convective outflow from developing thunderstorms. The research team was aware that the fire season in Colorado in 2012 was an active one [*Johnson et al*., 2014], with fires beginning in early June and that the air quality along the Front Range on the date of this flight was impacted by fire emissions. Thus, in addition to studying the convective outflow of the storms, research flights investigated the actively burning High Park fire, west of Fort Collins, which was first detected on 9 June [*Lang et al*., 2014] and was declared 100% contained on 30 June.

2. Methods

2.1. TOGA

The Trace Organic Gas Analyzer (TOGA) was deployed on the GV and used to measure a wide range of VOCs, including NMHCs, OVOCs, nitriles (BB tracers), and halogenated VOCs. The instrument is based on the concepts of earlier versions of the instrument previously described in the literature [*Apel et al*., 2010; *Hornbrook et al*., 2011]. A number of new species were measured by TOGA for this experiment including HCN and acrolein, so these, along with the third fire tracer ACN, are described in some detail here along with a basic description of the instrument operation.

The system is composed of the inlet, cryogenic preconcentrator, gas chromatograph, mass spectrometer, zero air/calibration system, integrated electronics, and data system. All processes and data acquisition are computer controlled. Three traps are used: a water trap, an enrichment trap, and a cryofocusing trap with silanized glass wool in the enrichment trap and open tubes for the water trap and cryofocuser. All tubing was 1/16 inch Silonite™ tubing (Entech Instruments, Inc., Simi Valley, CA). For the enrichment cycle, the water trap and enrichment traps were set to −25°C and −130°C, respectively. The flow rate during sampling was 25 mL/min and the sample collection time was 35 s, yielding a sample volume of 14.6 mL. Following this, the enrichment trap was heated at 25°C/s from −130°C to 100°C and transferred with He carrier gas at 1 mL/min to the cryofocus trap which was cooled to −130°C. The cryofocusing trap was then heated, also at 25°C/s, from the cold set point to +100°C, in the presence of 1 mL flow of He carrier gas, thereby injecting the sample onto the custom-designed gas chromatograph (GC). The GC is fitted with a Restek MTX-624 column (ID = 0.18 μm, length = 8 m). The initial GC oven temperature of 25°C was held for 10 s followed by heating to 120°C at a rate of 110°C min^{-1}. The oven was then immediately cooled to prepare for the next sample. Sample processing time was 2 min.

An Agilent 5973N Mass Spectrometer with a fast electronics package was used for detection using the single ion mode set to m/z = 27 for HCN, 41 for ACN, and 56 for acrolein. The system was operated in standard electron ionization mode operated at 70 eV. A nonstandard three-stage pumping system was used consisting of a Varian 301 turbomolecular pump, an Adixen (model MDP 5011) molecular drag pump, and a 28 V DC KNF-Neuberger diaphragm rough pump.

Table 1. Summary of Measurement Techniques Aboard the NASA DC-8 and NSF/NCAR GV Aircraft Used in the Analyses

Species	Technique	Reference
	DC-8 Aircraft	
NO	NO/O_3 chemiluminescence (CL)	*Ryerson et al.* [2000]
NO_2	UV photolysis followed by NO/O_3 CL detection	*Pollack et al.* [2012]
OH	Laser-induced fluorescence-ATHOS	*Brune et al.* [1998]
HCN	Chemical ionization mass spectrometry	*Crounse et al.* [2009]
ACN	Proton transfer reaction mass spectrometry	e.g., *de Gouw et al.* [2006]
CO	IR spectroscopy	*Eisele et al.* [2003]
PANs	Chemical ionization mass spectrometry	*Slusher et al.* [2004]
VOCs[a]	Whole Air Sampler (WAS)-gas chromatography/flame ionization detection/mass spectrometry	*Colman et al.* [2001]
	GV Aircraft	
O_3	NO/O_3 CL	*Ridley et al.* [1992]
NO	NO/O_3 CL	*Ridley and Grahek* [1990]
NO_2	UV photolysis followed by NO/O_3 CL detection	*Ridley and Grahek* [1990]
CO	Vacuum UV fluorescence	*Gerbig et al.* [1999]
VOCs[b]	In situ gas chromatography mass spectrometry-TOGA	*Apel et al.* [2012]
ACN[b], Acrolein[b]	TOGA	*Apel et al.* [2012]
HCN[b]	TOGA	Apel et al., in preparation
H_2O_2, CH_3OOH	CIMS	Silwal et al., in preparation
HCHO	Difference frequency generation spectrometry-CAMS	*Weibring et al.* [2010]

[a]WAS canister sampling frequency and integration time varied depending on location and altitude but averaged approximately one integrated sample every 4 min.
[b]TOGA VOCs were integrated for 35 s every 2 min.

A custom-fabricated catalytic-clean air generator/dynamic dilution system, referred to herein as the Zero Air/Calibration System (ZA/CS) [*Guenther and Hills*, 1998; *Apel et al.*, 2003], was used for system blanks and calibrations. The system contains two calibrated mass flow controllers, one for the calibration mix (0–30 $cm^3\,min^{-1}$ STP) and one for the diluent gas (0–10 standard liters per minute) and is used to dilute mid-ppbv to low-ppmv gas phase standards to ambient-level mixing ratios. This arrangement yields accurate (±1%) and precise (±1%) gas delivery. The diluent gas is ambient air that is drawn in through an inlet and scrubbed via catalytic oxidation (platinum on alumina at 425°C). This arrangement allows the diluent gas to mimic the humidity levels and permanent gas mixing ratios of the air masses under investigation.

ACN and acrolein were prepared in known amounts in a high-pressure Al cylinder, and this was used for calibrating through the ZA/CS both in the laboratory and during flight. The total uncertainty was determined by summing in quadrature: (a) the preparation uncertainty of the gravimetric standard (5%), (b) the uncertainty in intercomparing the mixes with other gravimetric standards (6%), (c) the uncertainty in replicate determinations from various days (4%), and (d) uncertainty associated with dilution of the standards (2%). Hence, the expanded uncertainty expressed at the 95% confidence limit for each compound concentration was determined by the expression

$$2\left(a^2+b^2+c^2+d^2\right)^{1/2} \quad (1)$$

or (±9%).

The options for calibrating HCN are limited because of the extreme toxicity of the molecule. The only readily available option is a permeation tube (PT). Thus, a PT containing liquid HCN (stabilized by a minute amount of sulfuric acid) and having a certified stated permeation rate of 317 ng min^{-1} at 30°C (KinTek Corporation) was used as the reference gas to calibrate the system in the laboratory. The permeation rate was checked in our laboratory by a high-precision Mettler AT261 balance and was found to be 317 ± 2 ng min^{-1}. A two-step dilution was necessary to reduce the permeation tube output to ambient levels. All flows were checked with calibrated BIOS DryCal™ flow meters to within 2% uncertainty. Using a similar approach as above, the total uncertainty at the 95% confidence limit which includes uncertainty in both dilution stages and replicate analyses (15%) is calculated to be ~±20%. Further details will be available in an upcoming publication (Apel et al., in preparation).

2.2. Other Measurements and Products Used

The instrumental techniques and references containing further details for the airborne measurements used in this analysis are summarized in Table 1. The chemiluminescence (CL) technique was used to measure

ozone (O_3), nitric oxide (NO), and nitrogen dioxide (NO_2) on both the GV [*Ridley and Grahek*, 1990; *Ridley et al*., 1992] and the DC-8 [*Ryerson et al*., 2000; *Pollack et al*., 2012] aircraft. The hydroxyl radical (OH) was measured aboard the DC-8 using laser-induced fluorescence (Airborne Tropospheric Hydrogen Oxides Sensor, ATHOS) [*Brune et al*., 1998]. Speciated nonmethane hydrocarbons (NMHCs) and other VOCs were measured aboard the DC-8 aircraft with the Whole Air Sampler (WAS) [*Colman et al*., 2001]. HCN and ACN were measured on the DC-8 with chemical ionization mass spectrometry [*Crounse et al*., 2009] and proton transfer reaction mass spectrometry [e.g., *de Gouw et al*., 2006], respectively. PAN and PPN were measured on the DC-8 with chemical ionization mass spectrometry [*Slusher et al*., 2004] and were not measured on the GV platform. Carbon monoxide (CO) and formaldehyde were measured aboard the GV aircraft via vacuum UV resonance fluorescence [*Gerbig et al*., 1999] and difference frequency generation spectrometry (Compact Atmospheric Multispecies Spectrometer, CAMS) [*Weibring et al*., 2010] techniques, respectively. Carbon monoxide was measured on the DC-8 with differential midinfrared spectroscopy [*Eisele et al*., 2003].

Satellite-borne visible images of the storm clouds are from GOES 13 (http://www.nasa.gov/mission_pages/goes-n/index.html#.U4dxJygrd3M). Ground-based measurements by the Colorado State University CHILL (http://www.chill.colostate.edu/w/CSU_CHILL) dual-Doppler and polarimetric radars, the National Weather Service Next Generation dual-Doppler Radar system (NEXRAD, http://www.roc.noaa.gov/WSR88D), the Northeast Colorado Lightning Mapping Array (NECLMA) [*Rison et al*., 1999], and measurements of cloud-to-ground (CG) lightning flashes from the National Lightning Detection Network (NLDN) (http://thunderstorm.vaisala.com) are used in the analysis presented here.

The full DC3 data archive with links to the airborne, satellite, lightning, and radar data products can be accessed at http://data.eol.ucar.edu/master_list/?project=DC3. In addition, all of the measurements from a given aircraft platform have been merged into composite databases and are available at the following web address: http://www-air.larc.nasa.gov/cgi-bin/ArcView/dc3?MERGE=1. These merges are available on different time bases including 1 s, 10 s, and 1 min. A majority of the data on each aircraft platform are reported every second, and thus, the 1 s merge combines these and other more slowly reported data into files for each flight as well as a combined full mission file. Ten second merges consist of averaging reported data over 10 s increments and 1 min merges consist of averaging the reported data over 60 s increments. Specific merges are also available for nonstandard sampling time bases such as TOGA and WAS canisters. For example, in the case of the TOGA merge, the database consists of averaging data collected from the faster measurements (e.g., 1 s time base measurements) over the TOGA sample collection time period which is 35 s every 2 min. Similarly for WAS, the faster measurements are averaged over the canister sample collection time.

2.3. Model

The NCAR master mechanism (MM) [*Madronich and Flocke*, 1999] was used to predict the chemical evolution from initial conditions observed in the outflow of the storm. The MM is a 0-D model with detailed gas phase chemistry consisting of ~5000 reactions among ~2000 chemical species combined with a mathematical solver. User inputs depend on the experiment being designed but include starting point mixing ratios (MRs) of species of interest, latitude, longitude, emissions, temperature, and pressure. The model as incorporated here computes the time-dependent chemical evolution of an air parcel initialized with known composition, assuming no additional emissions, no dilution, and no heterogeneous processes [*Madronich*, 2006]. Any input parameter may be constrained with respect to time. Photolysis rates are calculated using the tropospheric ultraviolet-visible model [*Madronich and Flocke*, 1999] included in the code package.

3. Results and Discussion

3.1. Colorado Convection

The main objective of the 22 June 2012 flights was to study Colorado convection in coordination with the ground observations by the CHILL and NEXRAD radars, NECLMA, and soundings. The timing of convection initiation was uncertain, so the DC-8 and the GV takeoff times were set to enable the aircraft to perform other studies while waiting for convection to develop.

Figure 1 shows GOES 13 satellite images of three convective cells that were studied on 22 June. Figure 1a shows an isolated storm, the first convective cell investigated (image taken at 22 June 2012, 21:30 UTC);

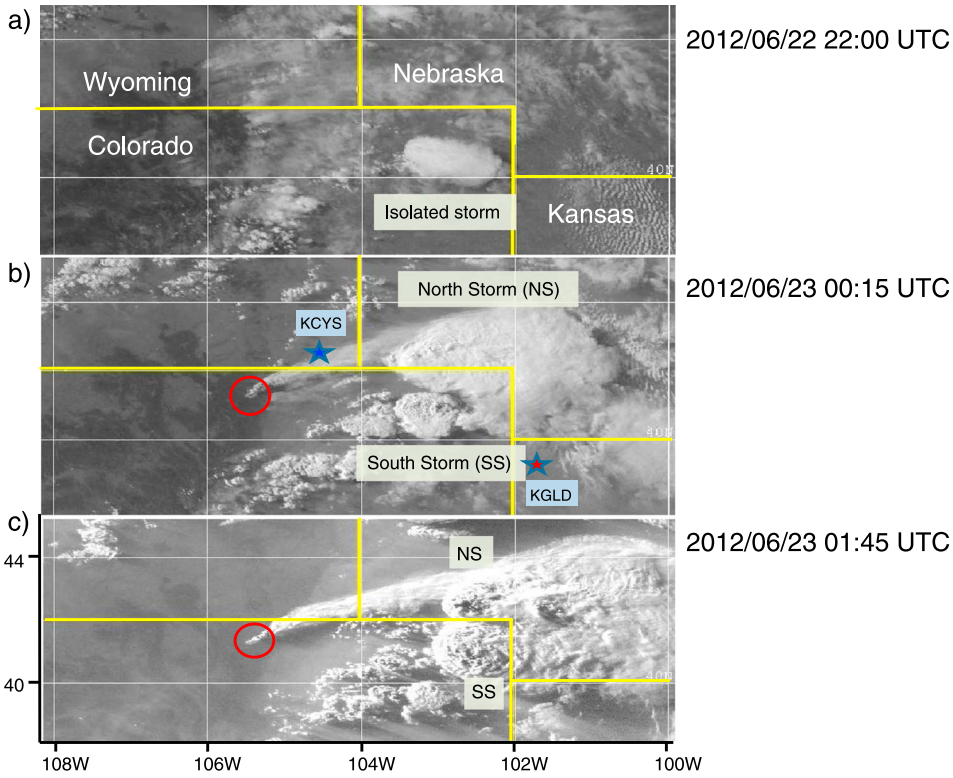

Figure 1. (a) GOES 13 satellite image from 22 June 2012 at 22:00 UTC. The isolated storm began developing at approximately 20:40 UTC. (b) GOES 13 satellite image from 23 June 2012 at 00:15 UTC showing development of the north storm (NS) and the south storm (SS). The Cheyenne, WY (KCYS), and Goodland, KS (KGLD), NEXRAD radar locations are shown. (c) GOES 13 satellite image from 23 June 2012 at 01:45 UTC showing further development of the NS and SS. The NS began forming at approximately 22 June 2012 22:00 UTC, and the SS began forming approximately 1 h later.

Figure 1b shows two other storms labeled north storm (NS) and south storm (SS) (image taken at 23 June 2012, 00:15 UTC) that developed later in the day and were subsequently probed by the research aircraft; Figure 1c shows the same two cells 1.5 h later. The High Park fire is visible in both Figures 1b and 1c (red circled area). As can be seen from the images, the smoke from the fire plume was ingested into the NS.

Figures 2 and 3 show Cheyenne, WY (KCYS), and Goodland, KS (KGLD), NEXRAD radar plots of the storm structures, respectively. They were captured within 15 min of the GOES 13 images in Figures 1b and 1c (the location of KCYS and KGLD are shown in Figure 1). Figure 2 indicates vigorous convective cells with peak reflectivities up to 60 dBZ. Echo tops (Figure 2a) are in excess of 12 km (although the large range from the radar to the storm core means that echo tops are approximate). A large forward anvil associated with light precipitation extends downshear. Figure 3 presents a radar depiction of the storm from the KGLD NEXRAD, approximately 90 min after the KCYS cross section in Figure 2. The storm continued to maintain strength, which is shown by the high reflectivities and echo tops. New storm cells were developing in the forward anvil 25–40 km ahead of the primary storm core.

The DC-8 flew from Salina toward the Wyoming border and then sampled the fire plume of the High Park fire between 2 and 7 km altitude above sea level (asl) at 20:44–20:59 UTC. The far left red circle in Figure 4a shows where the fire originated (NEXRAD image, the DC-8 flight track is shown in black with the flight direction to and from Salina shown by the arrows). The GV transited to Colorado from Salina KS in the clean FT (Figure 4a, white flight track superimposed over NEXRAD images with the flight direction to and from Salina shown by the arrows) and executed a low-level leg between 3.5 and 4 km asl (light blue oval in Figure 4a) on the Colorado Front Range. These low-altitude measurements (Figure 4b, time series trace), centered on about 21:00 h UTC, showed levels of HCN and ACN enhanced above tropospheric background (typically 100–150 pptv for ACN (e.g., this paper and *Aiken et al.* [2010]) and ~ 200 pptv for HCN (e.g., this

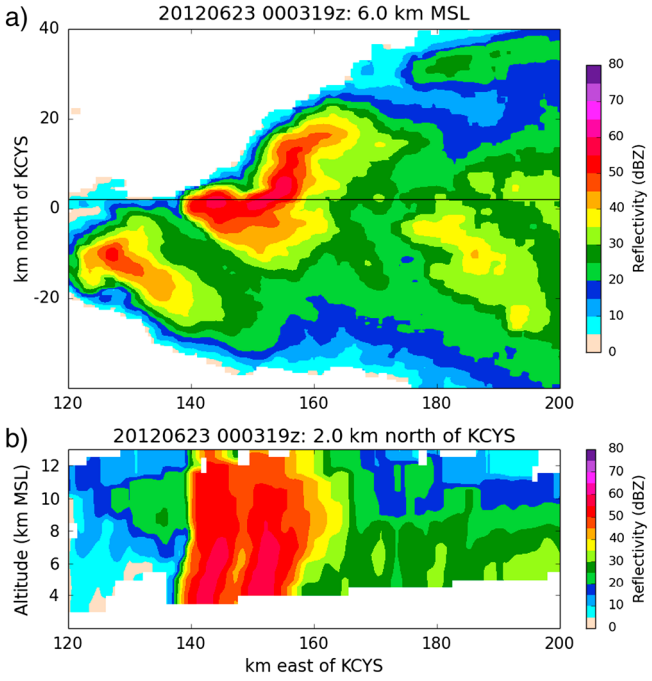

Figure 2. Reflectivity (dBZ) from the KCYS NEXRAD radar depicting the structure of the storm system at 0003 UTC 23 June 2012. (a) A CAPPI (constant altitude plan position indicator, horizontal cross section) of the storm at 6 km mean sea level; (b) a west-east cross section through the storm with the cross-section location indicated by the black line through Figure 2a. Horizontal distances are kilometers north-south and east of KCYS.

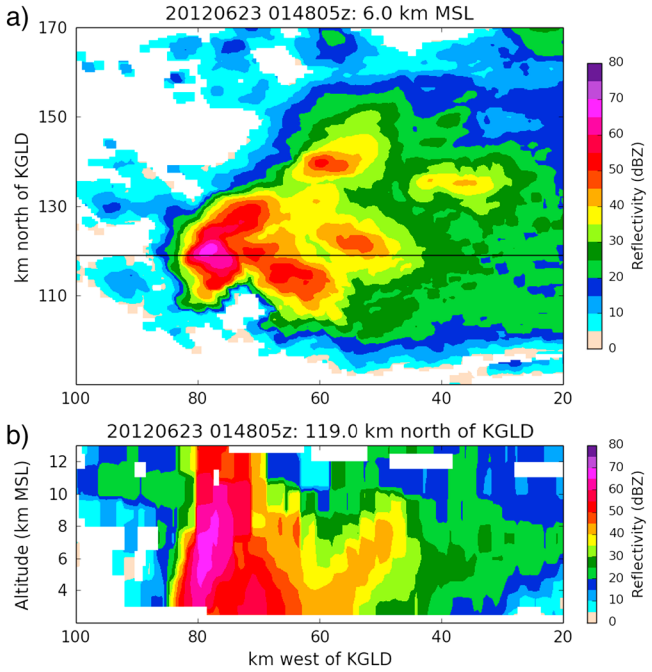

Figure 3. Similar to Figure 2 but showing the KGLD NEXRAD radar reflectivity of the SS at 0148 UTC 23 June 2012. Horizontal distances are kilometers north and west of KGLD.

paper and *Knighton et al.* [2009])) characteristic of a relatively well mixed air mass that had been influenced by BB. Acrolein was slightly enhanced, between 10 and 20 pptv. Following this, the GV ascended up to the storm outflow region at 11 km and from 22:15 to 23:30 interrogated the outflow of the isolated storm (shown in the satellite image in Figure 1a) that had developed near the Colorado-Nebraska-Kansas borders. The storm outflow was traversed several times, showing evidence of fire influence (Figure 4b) with enhanced HCN and ACN, though there was little if any enhancement of acrolein, indicating that the fire emissions sampled were not fresh.

Although the smoke plume trajectory from the active High Park fire (circled in red, Figures 1b, 1c, and 4a) is distinct on the day of the flights, this fire had been burning since 9 June and was impacting air quality throughout the Front Range. The data obtained from the isolated storm are consistent with sampling of lofted boundary layer emissions that included aged BB emissions that had accumulated over the previous days. There were a number of devastating fires in the summer of 2012 following an extremely dry winter, but the High Park fire was the only significant fire during the time period considered here.

As the isolated storm began to die, the north storm (NS) was forming (Figures 1b and 1c); remaining at a similar altitude (~ 11 km), the GV aircraft abandoned the isolated storm for the growing NS. NEXRAD Doppler radar and GOES 13 satellite images (not shown) indicate that this new storm began growing at approximately 22:05 UTC. GOES 13 and NEXRAD images (Figures 1b, 1c, and 2)

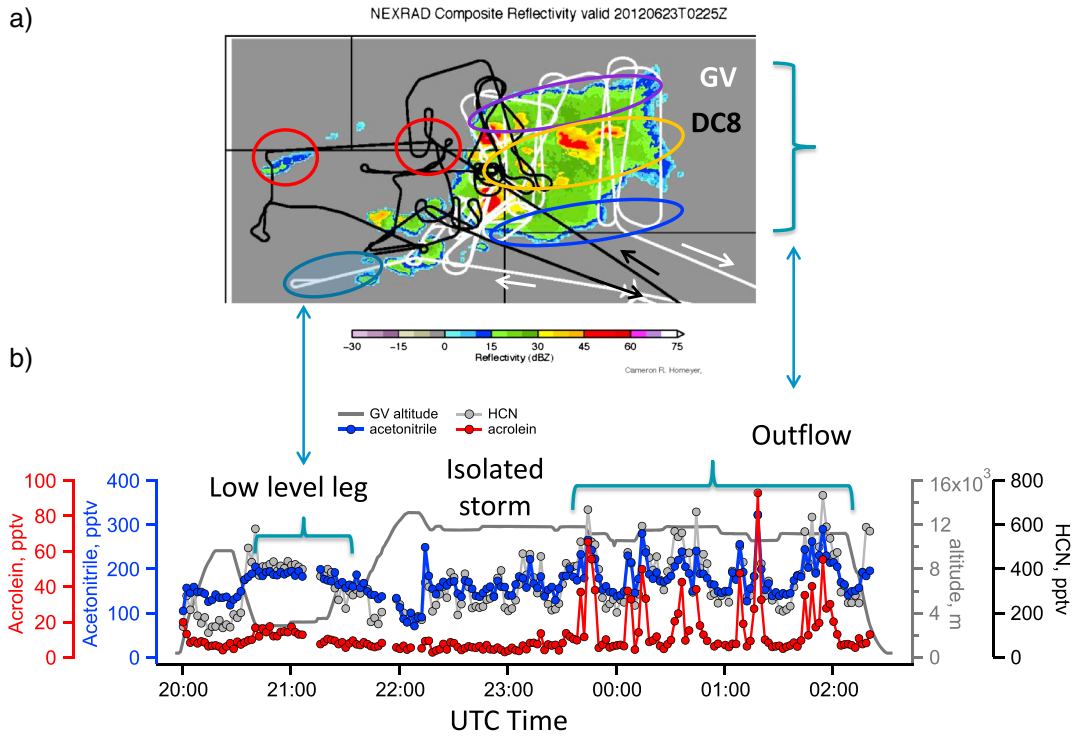

Figure 4. Results from the Colorado-Nebraska convection studied during the 22 June 2012 research flights. (a) NEXRAD image overlaid with DC-8 and GV flight tracks. The arrows indicate the direction of the flight paths. The far left red circle indicates the fire origin, and the further right red circle indicates where the DC-8 intercepted the High Park fire plume near the end of the research portion of the flight. The light blue oval indicates the region of the low-level leg executed on the Front Range. The purple oval indicates the approximate location of the NS outflow, the gold oval the SS outflow, and the blue oval indicates the region studied that was outside of the main outflow. (b) The corresponding time series of TOGA-measured fire tracers HCN, acetonitrile (ACN), and acrolein showing the approximate time range during which the low-level, isolated storm, and outflow legs were executed.

indicate the presence of a third storm cell (SS) that had begun to form at approximately 23:00 UTC and was reasonably well developed by approximately 23 June 00:00–00:15 UTC (Figure 1b). Inspection of the satellite images in Figures 1b and 1c shows the presence of these two cells in close proximity to one another, one centered just north of the Colorado-Nebraska border (NS) and one just to the south of the border (SS). In the NEXRAD image shown in Figure 2, the two separate cells are visible each with reflectivity $>$ 50 dBZ.

The high-reflectivity region in Figure 4a designates where the outflow from the NS and SS was sampled. Two distinct regions of the outflow, represented by the purple and gold ovals in Figure 4a, were sampled by several legs flown by the GV approximately orthogonal to the outflow of the storms. The purple oval area represents the approximate region where the GV sampled the outflow that was primarily from the NS. The gold oval area represents the approximate region where the GV sampled in outflow primarily from the SS. The blue oval area on the south side of the storms in Figure 4a represents the sampled region that was just outside of outflow from either storm and corresponds with the portion of the time series in Figure 4b when the three fire tracers are at their minimum values in the section of the time series labeled "Outflow." The black flight track in Figure 4a indicates where the DC-8 also measured the outflow of these storms on the western edge.

Figure 5 reproduces the NEXRAD composite reflectivity with the DC-8 and GV flight tracks overlaid (Figure 5a) and shows HCN from the DC-8 (Figure 5b) and acrolein and HCN from the GV (Figures 5c and 5d, respectively). The plots are color coded with respect to the species of interest, and relative sizes of the points indicate the altitude with low-altitude points smaller and high-altitude points larger. The DC-8 HCN plot indicates where the fire plume was intercepted. Recall that the first intercept was at 2–7 km early in the flight (high HCN values from the fire origin and along the CO-WYO-NE border) and the second intercept at ~ 7 km near the end of the

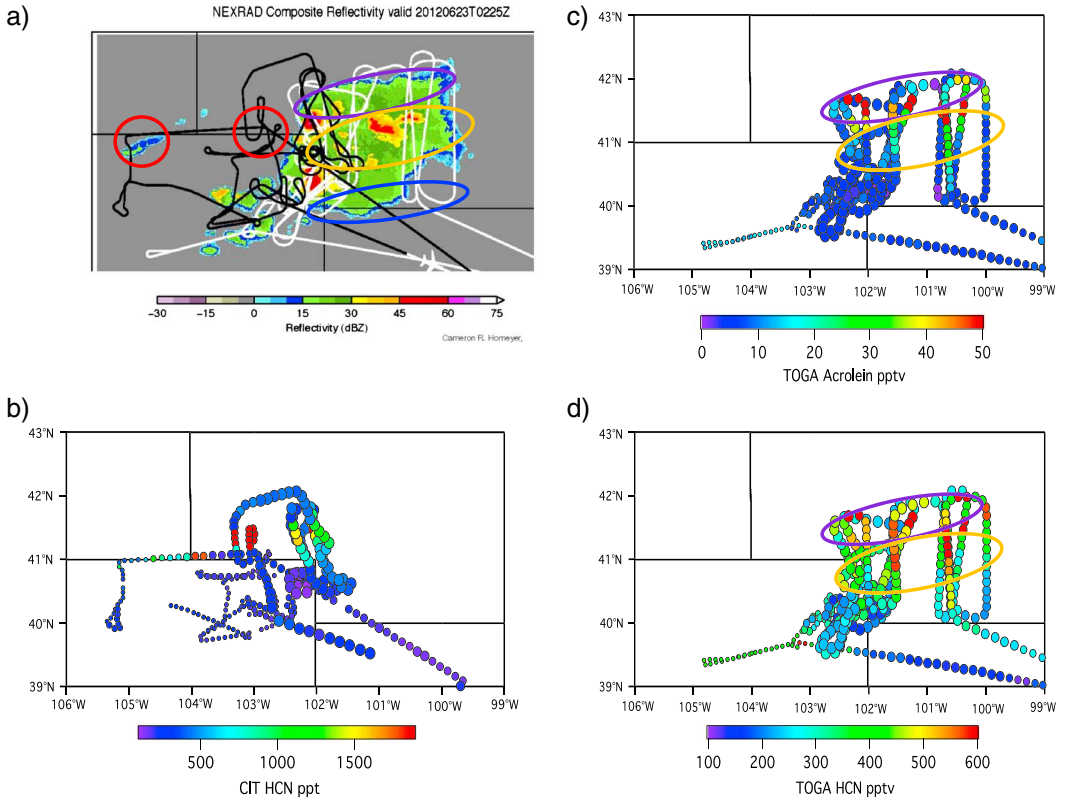

Figure 5. (a) NEXRAD image with flight tracks overlaid as in Figure 4a: (b) DC-8 HCN measurements for the 22 June flight taken from the DC-8 1 min data merge. The flight track is color coded with HCN mixing ratios, and the size of the data points (circles) scales with altitude; the smaller circles representing low altitude and larger circles high altitude. (c) GV acrolein measurements for the 22 June flight taken from the GV 1 min data merge. The flight track is color coded with acrolein MRs, and the markers are scaled by altitude, with the smaller circles representing low altitude and larger circles high altitude; (d) GV HCN measurements plotted as for Figure 5c.

flight (Figure 5a, red circle centered approximately at 103.1°W, 41.2°N); in the time between the two passes, the fire had flared up to burn a new section of terrain. Very high HCN values were obtained (> 5000 pptv) during the second pass (Figure 5b, full scale not shown in figure) indicating that thick smoke was sampled. Note that acrolein is most enhanced in the NS (Figure 5c), whereas the longer-lived HCN is enhanced in both the NS and the SS (Figure 5d) but with the NS having slightly higher average values for both HCN and ACN (see Table 3 for values averaged over the points sampled in and out of the outflow). The acrolein data are consistent with the visual satellite images in Figures 1b and 1c showing that the fresh High Park fire emissions were ingested into the NS. Radar images (not shown) indicate that the smoke from the High Park fire was ingested into the convective column of the storm at an altitude of 5–8 km, consistent with the DC-8 data.

Figure 6 shows several other tracers displayed in the same way as in Figure 5. The outflow from both the NS and the SS exhibits highly elevated values (relative to surrounding nonoutflow data) for the boundary layer tracers O_3, CO, formaldehyde, ACN, and *n*-butane at this altitude (~ 10 km) indicating efficient transfer via the storms from the source region to the UT. NO and NO_2 (Figure 6 and Table 3) are higher in the SS, and it is clear from Figure 6 that NO is elevated in the outflow compared to the inflow. A separate analysis is being done on the lightning characteristics of both storms. The NS was initially bigger and was producing high flash rates (>200 flashes/min) early on, before the aircraft arrived. The south storm became much bigger later on, likely producing more lightning concomitant with more NO_x (as observed). Unfortunately, both storms were well out of CHILL's range after about 01:00 UTC. CO is higher on average in the NS outflow as fresher BB emissions were entrained and subsequently sampled. The alkanes including *n*-butane (shown in Figure 6) are elevated in the outflow of both storms (slightly higher on average in the SS, Table 3) likely reflecting convection of boundary layer emissions from oil and natural gas operations which are

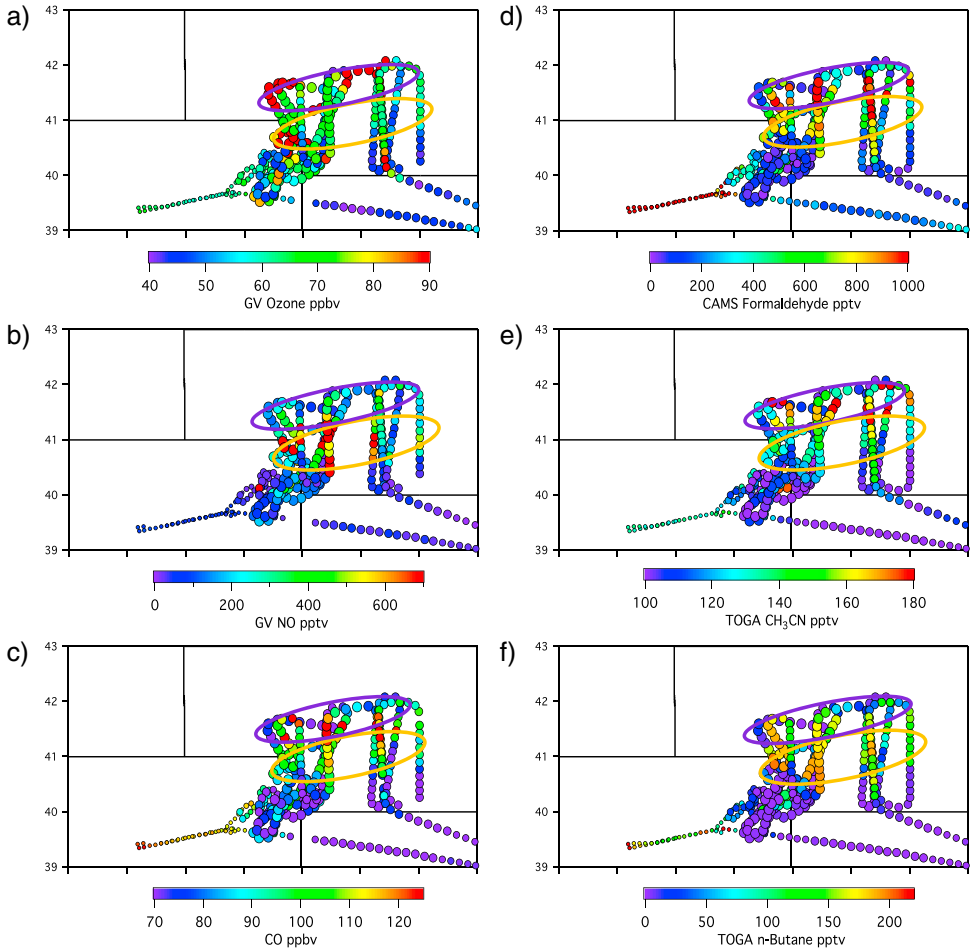

Figure 6. GV measurements along the flight track during the 22 June 2012 research flight plotted as for Figure 5c. (a) Ozone, (b) NO, (c) CO, (d) CAMS formaldehyde, (e) ACN, and (f) *n*-butane.

prevalent in the area [*Gilman et al*., 2013]. The alkenes (Table 3) are higher in the NS which is expected for a more BB-impacted air mass.

3.2. Air Mass Age and Normalized Excess Mixing Ratio Calculations

Characteristic species, including toluene and benzene, are emitted directly by fires. Both toluene and benzene react with the hydroxyl radical (OH) but at different rates. This can be used to obtain information on the approximate photochemical age of an air mass impacted by BB. If the ratio of benzene to toluene near the fire source ($t = 0$) is known and the integrated [OH] is known from the time of emission until the time of detection, then the photochemical age of the air mass can be determined from [*Gelencsér et al*., 1997; *de Gouw et al*., 2005]

$$\Delta t = \frac{1}{[\mathrm{OH}][k_{\mathrm{toluene}} - k_{\mathrm{benzene}}]}\left[\ln\left(\frac{[\mathrm{toluene}]}{[\mathrm{benzene}]}\right)_{t=0} - \ln\left(\frac{[\mathrm{toluene}]}{[\mathrm{benzene}]}\right)\right] \quad (2)$$

Although the rate constants of benzene and toluene with OH are well known, they vary with temperature. At temperatures experienced within a typical fire (600–1000 K), the ratios of the rates of benzene:OH to toluene:OH are near unity, but outside of the fire itself toluene reacts significantly faster than does benzene; at 298 K, toluene reacts 5 times faster than benzene, and at temperatures experienced in the outflow, approximately 230 K, toluene reacts 11 times faster. Complicating the picture somewhat here, the full integrated [OH] over the time since emission is difficult to know exactly because in fire plumes and in convective systems the photolysis frequencies (*J* values) vary rapidly. However, the residence time in the convective system is relatively short compared to the total smoke age, so its overall effect on the OH exposure is small. Put simply, the more

Table 2. Plume Intercepts and Normalized Excess Mixing Ratios (pptv(*x*) ppbv^{-1} CO) Determined by Orthogonal Distance Regression (ODR) for the GV Data in the NS Outflow and for the DC-8 Data Obtained During Fire Plume Intercepts and NS Outflow[a]

	HCN				ACN				Acrolein			
	NEMR	±[b]	r^2	No. of Points	NEMR	±	r^2	No. of Points	NEMR	±	r^2	No. of Points
					GV							
Outflow intercept NS times:												
22 June 2012 23:32 to 23 June 2012 2:02	6.84	0.98	0.74	19	1.83	0.28	0.68	19	1.41	0.29	0.49	19
					DC-8							
Fire plume intercepts:												
22 June 2012 20:44:30–20:59:30	2.74	0.25	0.90	15	1.02	0.14	0.78	16				
23 June 2012 01:42:30–2:01:30	6.65	0.50	0.92	18	2.61	0.13	0.89	20				
Combined fire plume intercepts	6.95	0.48	0.87	33	2.55	0.18	0.85	36				
Outflow intercept NS times:												
23 June 2012 00:34:30–01:30:30	7.27	0.29	0.93	39	2.57	0.08	0.96	39				

[a]The GV data are from the DC3 archive TOGA merge, and the DC-8 data are from a 1 min merge.
[b]Standard error in the ODR fit.

photochemically aged fire plumes should have progressively smaller toluene/benzene ratios. This trend can be used to compare relative photochemical ages of NS outflow (i.e., where acrolein is significantly enhanced) versus SS outflow (acrolein not significantly enhanced). An initial ratio of 0.69 for toluene to benzene was obtained for the High Park fire from the DC-8 WAS observations that intercepted fresh smoke from the fire on 22 June 2012 at 20:44–20:59 UTC and 0.68 when the DC-8 intercepted the plume once again, later in the flight on 23 June 2012 at 01:42–02:01 UTC. This ratio falls within the range of values found in the literature for this type of forest fire [*Friedli et al.*, 2001; *Akagi et al.*, 2011]. Using the observed toluene/benzene ratio, an observed average daytime OH mixing ratio of 3.7×10^6 molecules cm^{-3} and a temperature of 260 K for the fire outflow (average temperature measured while traversing the plume), the estimated photochemical ages of the air in the NS (purple area, Figures 4–6) and SS outflow (gold area Figures 4–6) are 8 and 15 h, respectively. The photochemical lifetime of acrolein under these conditions ($K_{OH} = 2.36 \times 10^{-11}$ [*Magneron et al.*, 2002]) is 3.2 h. Thus, the relative age of the two portions of the outflow is consistent with our fire tracer (acrolein) measurements in that the older outflow is too aged to have maintained the MRs seen in the less aged outflow.

Emission ratios (ERs) or enhancement ratios (EnRs, also referred to as normalized excess mixing ratios, NEMRs) are commonly used terms to quantify the emissions from, and atmospheric impact of, BB. An emission ratio (ER) is the molar ratio between two emitted compounds measured at a fire source and is generally reported as $\Delta[X]/\Delta[Y]$ where $\Delta[X]$ and $\Delta[Y]$ refer to mixing ratios of the two species in the fire plume minus the mixing ratio of those species in background air. *Y* is generally a long-lived fire tracer such as CO, which is used in this analysis. By definition, ERs refer only to fresh emissions, whereas an NEMR can refer to the enhancement of a compound *X* measured downwind from a fire with respect to the enhancement of a fire tracer *Y*, also reported as $\Delta[X]/\Delta[Y]$.

NEMRs were calculated for the three fire tracers for the GV NS data (times shown in Table 2) using orthogonal distance regression (ODR) fits. Table 2 shows the results from this analysis: the NEMRs relative to CO are found to be 6.84 ± 0.98, 1.83 ± 0.28, and 1.41 ± 0.29 (pptv ppbv^{-1}) for HCN, ACN, and acrolein, respectively. The r^2 value for the standard linear regression fit to the data is included to provide further information on the goodness of fit.

From the DC-8 passes through the fire plume at two different times (Table 2) on 22/23 June, NEMRs were found to be 2.74 ± 0.25 and 1.02 ± 0.14 for HCN and ACN, respectively. In the time between the two passes, the fire had flared up burning a new section of terrain. For the second pass the NEMRs were found to be considerably different, 6.65 ± 0.50 and 2.61 ± 0.13 for HCN and ACN, respectively. The modified combustion efficiency (MCE) was calculated for each of the two fire intercepts and was found to be 0.91 for the data obtained on the first and 0.94 for the data obtained on the second. An MCE of 0.99 indicates pure flaming combustion, while MCEs between 0.65 and 0.85 are considered to indicate pure smoldering combustion, and MCEs between 0.85 and 0.99 indicate a mixture of flaming and smoldering [*Akagi et al.*, 2011]. Thus, the plume encountered during the second pass was in a more flaming stage than in the first pass and may have burned different vegetation types, either or both of which affected the NEMRs. In between, the DC-8 also

measured the outflow of the NS finding NEMRs of 7.27 ± 0.29 and 2.57 ± 0.08 for HCN and ACN, respectively, entirely consistent with the second direct fire pass.

The TOGA HCN and the CIT HCN values agree well. There are possible differences between the TOGA and PTR-MS ACN data, but this cannot be determined from these data alone. The HCN NEMRs from this work fall within the ranges found in more recent literature, 2.4–12.8 [*Yokelson et al*., 2007a, 2007b, 2009; *Simpson et al*., 2011; *Akagi et al*., 2011; *Hornbrook et al*., 2011; *Le Breton et al*., 2013] but are higher than earlier reported values, which are in the range of 0.43–1.5 [*Andreae and Merlet*, 2001]. The ACN NEMRs also fall within the ranges found in the literature, 1.1–4.3 [*Andreae and Merlet*, 2001 (conversion done by authors of this paper from emission factors (EFs) in g kg^{-1} dry weight burned, given in reference); *de Gouw et al*., 2006; *Yokelson et al*., 2007a, 2009; *Warneke et al*., 2009; *Hornbrook et al*., 2011; *Akagi et al*., 2011; *Simpson et al*., 2011]. No ERs or NEMRs have previously been reported for these compounds in this area of the U.S.

The measured NEMR for acrolein is somewhat higher than the ER reported by *Andreae and Merlet* [2001] for extratropical forest BB emissions (0.84). Emission ratios using a PTR-MS for mass 57 representing acrolein (plus possibly other species at the same mass) have also been reported in two recent studies; *Kostenidou et al*. [2013] performed a controlled burn study of olive tree branches and derived an ER of 6.4 pptv acrolein $ppbv^{-1}$ CO (conversion done by authors from EFs), and *Warneke et al*. [2011] derived ERs (pptv acrolein $ppbv^{-1}$ CO) of 0.55, 1.39, and 1.56 for mass 57 using a PTR-MS in a controlled laboratory burn experiment for fuels collected to represent regional vegetation from the southwestern U.S., southeastern U.S., and some pine, spruce, and fir samples, respectively, showing reasonable agreement with the TOGA data. *Akagi et al*. [2011] report an ER value of 3.5 pptv acrolein $ppbv^{-1}$ CO for tropical forest burning. *Yokelson et al*. [2013] report an ER (pptv acrolein $ppbv^{-1}$ CO) of 2.26, quantified with the Fourier transform infrared technique. This value is the average for prescribed fires in pine forest understory and semiarid shrub land, and fires in coniferous canopy fuels, but encompasses a very large variability over many measurements.

Although weakly soluble, it is unlikely that acrolein is significantly scavenged in the storm because formaldehyde, which is 3 orders of magnitude more soluble than acrolein [*Sander*, 1999], is typically scavenged on the order of only 50% in storms studied thus far during DC3 (A. Fried et al., private communication, 2014). In our study some of the acrolein will have reacted relative to CO before sampling but it is also likely that some acrolein has been produced from precursors, chiefly 1,3-butadiene, which is known to be emitted from fires [*Friedli et al*., 2001, *Akagi et al*., 2011] but not reported in the DC3 data archives; based on known emission ratios, reaction rates [*Magneron et al*., 2002], and product yields [*Sprengnether et al*., 2002], we estimate that 1,3-butadiene emitted at the fire source contributes up to 15% of the total acrolein observed. This secondary production will effectively extend acrolein's lifetime slightly.

3.3. Box Modeling

An objective of this study was to use the NCAR master mechanism (MM) model to predict the chemical evolution of the plume in the UT outflow from the storms and, specifically, to quantify the ozone production potential. The model offers an opportunity to examine chemical transformations of these isolated outflows at a level of detail that is impractical to implement in current 3-D models.

Three primary model runs were done using a full suite of VOC, NO_x ($NO + NO_2$), CO, O_3, etc., MRs to initiate the model (Table 3): scenario (1) initialized with values obtained in the NS (purple ovals, Figures 4–6); scenario (2) initialized with values obtained within the SS (gold ovals in Figures 4–6); and scenario (3) initialized with values obtained outside of the outflow (blue ovals, Figures 4–6). Effects of dilution are not considered here. All starting point mixing ratios were taken from the NASA merge file (http://www-air.larc.nasa.gov/cgi-bin/ArcView/dc3-seac4rs) for the GV and DC-8 aircraft platforms. Most of the VOC data were taken from the GV TOGA data with the exception of ethyne, ethene, ethane, and propene which were taken from the DC-8 UCI WAS measurements. It should be noted here that although a significant number of VOCs were identified and quantified, studies have shown that there are numerous VOCs present in ambient atmospheres and the suite measured here is not all inclusive [*Lewis et al*., 2000; *Akagi et al*., 2011; *Yokelson et al*., 2013]. Research groups responsible for the other measurements are shown in Table 1.

Scenario 1 data encompass the outflow from the NS that is influenced by fresh emissions from the High Park fire. The average initial mixing ratios of NO_2 and NO for the NS are 294 and 314 pptv, respectively, and are

Table 3. Average Values for the NS and SS Outflows and for Values Outside of the Outflow in the Free Troposphere

Parameter	NS Value	SS Value	Out of Storm	Units
Temperature	226.28	225.18	229.64	K
Pressure	237.51	230.99	254.42	hPa
Altitude	10.70	10.88	10.80	Km
Latitude	41.54 (41.22–41.99)	40.98 (40.64–41.24)	40.29	deg
Longitude	101.1 (100.0–102.4)	101.1 (100.0–102.3)	100.70	deg
H_2O	256	223	268	ppmv
O_3	64	65	52	ppbv
NO_2	295	490	72	pptv
CO	110	103	73	ppbv
NO	314	646	37	ppbv
Methane	1831	1834	1806	ppbv
Ethyne (WAS)	238	152	60	pptv
Ethene (WAS)	445	191	0	pptv
Ethane (WAS)	1523	1496	1200	pptv
Propane (WAS)	517	556	50	pptv
n-butane (TOGA)	128	157	6	pptv
i-butane (TOGA)	55	67	2	pptv
Propene (TOGA)	158	56	7	pptv
i-butene (TOGA)	12	8	3	pptv
Isoprene (TOGA)	1	1	0	pptv
n-pentane (TOGA)	31	37	1	pptv
i-pentane (TOGA)	30	38	1	pptv
n-hexane (TOGA)	8	9	0	pptv
2-methylpentane (TOGA)	6	6	0	pptv
n-heptane (TOGA)	4	3	0	pptv
Benzene (TOGA)	52	31	7	pptv
Toluene (TOGA)	21	7	0	pptv
Ethylbenzene (TOGA)	4	1	0	pptv
CH_2O (CAMS)	815	657	40	pptv
Acetaldehyde (TOGA)	303	211	7	pptv
Propanal (TOGA)	21	13	2	pptv
Butanal (TOGA)	5	3	2	pptv
Methanol (TOGA)	2833	3258	490	pptv
Ethanol (TOGA)	105	123	30	pptv
Acetone (TOGA)	1712	1928	417	pptv
MEK (TOGA)	106	120	4	pptv
MACR (TOGA)	3	3	0	pptv
MVK (TOGA)	16	9	0	pptv
H_2O_2 (CIT)	237	217	270	pptv
CH_3OOH (CIT)	355	371	147	pptv
HCN (TOGA)	508	441	262	pptv
ACN (TOGA)	161	134	105	pptv
Acrolein (TOGA)	35	13	7	pptv
Methyl nitrate (WAS)	8	10	2	pptv
Ethyl nitrate (WAS)	5	5	3	pptv
Propyl nitrate (WAS)	1	1	1	pptv
Isopropyl nitrate (WAS)	7	8	5	pptv
Isobutyl nitrate (WAS)	10	12	9	pptv
3-PenONO_2 (WAS)	3	4	4	pptv
2-PenONO_2 (WAS)	5	6	2	pptv
3-Methyl-2-BuONO_2 (WAS)	3	4	2	pptv
PAN (GTCIMS)	298	254	200[a]	pptv
PPN (GTCIMS)	28	23	20[a]	pptv

[a]These values are estimated, not measured.

likely a result of both lightning-produced NO_x, fire, and anthropogenic NO_x that has been swept up from the fire-influenced boundary layer. Measurements of CG lightning flashes from the NLDN and the NECLMA show substantial lightning activity in the NS and the SS beginning at about 22 June 2012, 22:40 UTC and continuing over the next several hours. Measurements of NO_x from the DC-8 while sampling the High Park fire show

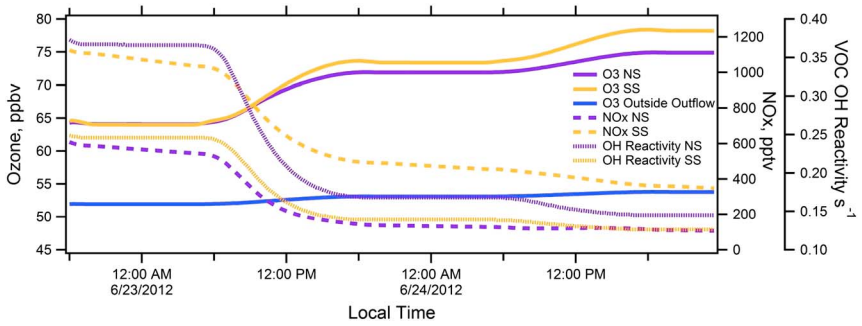

Figure 7. NCAR master mechanism initialized with the average MRs of species for the NS, SS, and outside the outflow (taken from Table 3).

that the fire produced substantial NO_x (first pass: 22 June 2012, 20:44 UTC–20:59 UTC, $NO_2 > 500$ pptv, $NO > 80$ pptv, second pass: 23 June 2012 01:42–02:01 UTC, $NO_2 > 2000$ pptv, $NO > 200$ pptv), but only a fraction of it was entrained into the storm. The initial average mixing ratios of NO_2 and NO for the SS are 490 and 646 pptv, respectively, and also likely result from a variety of sources but are primarily due to lightning because the boundary layer (inflow) NO_x values are only ~ 200 pptv as measured by the GV during the low-level leg earlier in the flight.

Figure 7 shows O_3, NO_x, and VOC OH reactivity results from the MM runs for all three scenarios with initial conditions for each given in Table 3. The SS produces the most ozone over a period of 2 days (gold trace, color scale consistent with the previous figures), starting from an initial value at $t = 0$ (the box model $t = 0$ corresponds to 6:00 P.M. local time) of 64.6 ppbv ozone and ending with 78.2 ppbv ozone (~ 14 ppbv). The NS initial condition MR is 64.3 ppbv ozone, and after 2 days of processing a MR of 74.9 ppbv (purple trace) is predicted. Thus, a lower amount of O_3 production is predicted (~ 11 ppbv) for the NS versus the SS despite the fact that the NS is much more impacted by fresh BB emissions. Ozone mixing ratios are also shown for outside the outflow (51.9 ppbv) showing that (1) both the NS and SS have enhanced initial ozone MRs compared to the background showing that ozone has already been produced in these air masses and (2) very little ozone is produced in the background air over the 2 day period. Also plotted in the graph is the time evolution of both NO_x and VOC OH reactivity. Not surprisingly, the average VOC OH reactivity is higher (0.37 s^{-1}) in the NS (entrained fresh BB emissions) compared to the SS (0.25 s^{-1}). However, because of LNO_x, the initial NO_x mixing ratio is substantially higher in the SS (1125 pptv) compared to the NS (609 pptv). Following the predicted chemical evolution from $t = 0$ (6:00 P.M. local time) for each storm, ozone stays constant during the night, the following day (23 June) the Sun rises and reactions of NO_x (see paragraph below for more details) and VOCs ensue resulting in rapid depletion of the precursors and significant ozone formation. However, enough precursors remain for both storms on the following day (24 June) to once again produce a response in the ozone mixing ratio.

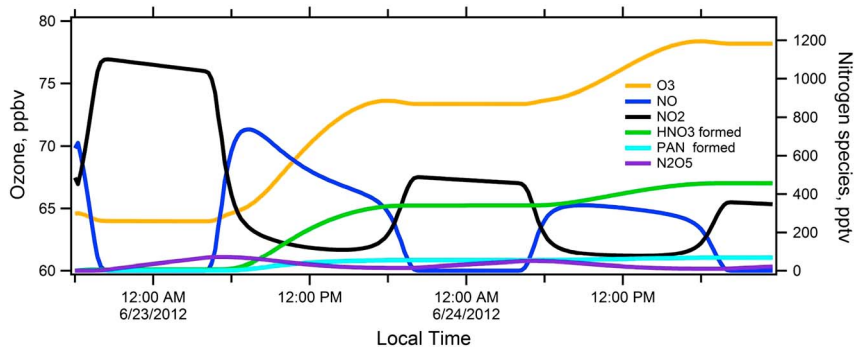

Figure 8. NCAR master mechanism initialized with the average MRs of species for the SS (Table 3) showing the evolution of important nitrogen-containing species.

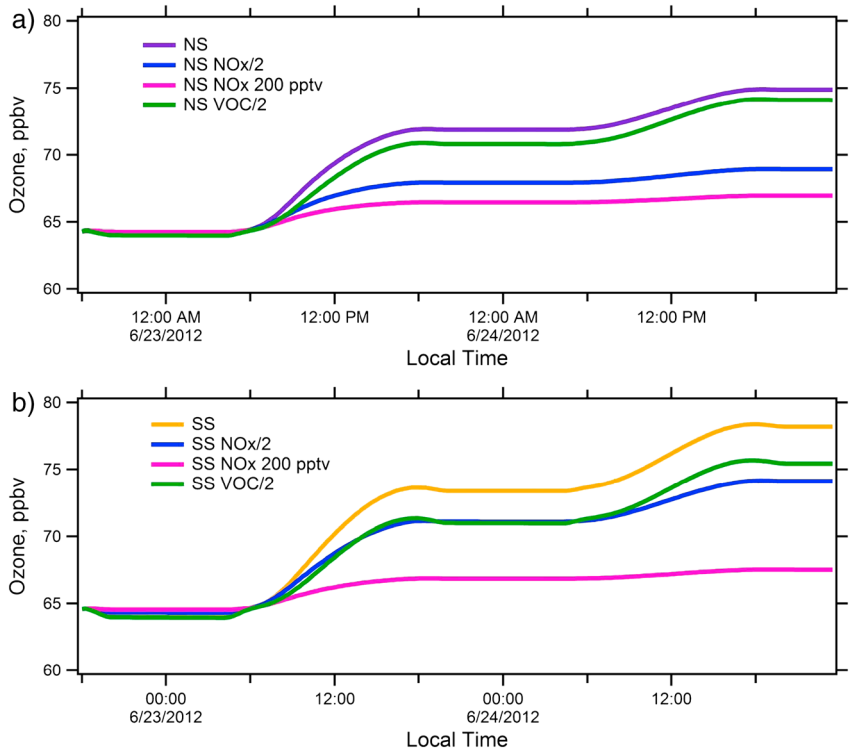

Figure 9. NCAR master mechanism initialized with the average MRs of species for the (a) NS and (b) SS (Table 3).

Figure 8 shows results for the chemical evolution of ozone and important nitrogen-containing species for the SS. Following the progression of the photochemistry from the initial local Sun time (6:00 P.M. local time), NO is converted to NO_2 at night. Nighttime reactions ($NO_2 + O_3 \rightarrow NO_3$) followed by $NO_2 + NO_3 \leftrightarrow N_2O_5$ produce N_2O_5 in modest amounts (~40 pptv, SS, 25 pptv, NS). When the Sun rises, photochemical reactions ensue. NO_2 quickly photolyzes to produce NO + O and HNO_3 and PAN begin to form. The rate of O_3 production falls off as more NO_x is sequestered into the PAN and HNO_3 reservoirs. During the most vigorous production of ozone, which occurs on the following day (23 June) after sunrise, [N_2O_5] is less than 5% of [NO_x] in either storm indicating that the impact of this channel on the magnitude of next-day ozone production is expected to be minor.

For outside the outflow, substantially less NO_x (NO = 37.5 ppbv and NO_2 = 71.6 ppbv) and fewer oxidant precursors are present, resulting in minimal ozone produced in this scenario.

To investigate the factors contributing to the predicted ozone formation in the outflow, sensitivity tests were run with the MM. Figure 9 shows the results of these tests with the NS results shown in Figure 9a and the SS results in Figure 9b. The trace color annotation is identical for both Figures 9a and 9b except for the unperturbed initial condition traces in the figures which are consistent with previous figures (purple for the NS outflow and gold for the SS outflow). The purple trace in Figure 9a and the gold trace in Figure 9b show the evolution of ozone from the actual initial conditions as was previously shown in Figure 7. The dark blue trace has identical initial conditions except that NO_x was halved. For the NS, halving the NO_x results in a reduction of O_3 formation of 56% over the course of 2 days, whereas in the more NO_x rich SS, halving the NO_x results in a decrease of only 30%. Reducing the NO_x to 200 pptv (which is the amount of NO_x measured in the BL) results in dramatically less ozone produced in both cases (pink trace) with the NS producing 75% less ozone and the SS producing 78% less ozone under these conditions. Reducing the VOC OH reactivity by a factor of 2 results in only a 7% reduction in ozone for the more VOC rich NS but a 20% decrease in the less VOC rich SS. The more VOC rich NS is less sensitive to changes in VOCs than the less VOC rich SS. The more NO_x rich SS is less sensitive to changes in NO_x than the NS. Thus, if only BL NO_x (200 pptv) is convected into the storms (i.e., absence of fire produced NO_x or LNO_x), then very little ozone is predicted to be produced from either storm. It is clear that LNO_x is the major contributor to predicted ozone formation in the SS outflow and is likely a significant contributor to predicted ozone formation in the NS outflow.

The GV aircraft flew the following day with the goal of finding the air mass that was convectively lofted in the Colorado storms the previous evening and sample its composition. However, little evidence of BB was found during the flight suggesting little or no connection to the previous day's sampling of the convective outflow. This was unfortunate as it could have provided a good test for our model results. However, the MM model previously has shown significant skill in predicting ozone production in the outflow from non-BB-impacted outflow events [*Apel et al.*, 2013] during DC3, lending confidence that the modeling results here have merit although with the caveat that even using the detailed chemical representation in the MM, not all initial species and not all reactions are represented.

As we have shown, this case involves the entrainment of both fresh and more aged BB emissions along with other boundary layer emissions into convective cells where lightning is producing substantial NO_x. Previous model estimates of ozone production rates for midlatitude convection not impacted by biomass burning range from 4 to 15 ppbv/d [*Pickering et al.*, 1990, 1992], depending on boundary layer composition and lightning flash rate production of NO_x. The results here predict 8 ppbv/d (first day) for the NS and 10 ppbv/d (first day) for the SS, both of which were impacted by BB. A number of studies have examined ozone production from fires [e.g., *Pfister et al.*, 2006, 2008; *Jaffe and Wigder*, 2012, and references therein; *Singh et al.*, 2012; *Jaffe et al.*, 2013], which is determined largely by the emissions from the fire that constitute the chemical potential for ozone formation and the actinic flux and temperature which determine the rate at which ozone is formed; aerosols can also play a role [*Konovalov et al.*, 2012]. Most but not all observations have shown that ozone is produced from fires but with highly varying yields. A variety of models, from global [e.g., *Martin et al.*, 2002; *Pfister et al.*, 2006, 2008; *Nassar et al.*, 2009; *Alvarado et al.*, 2010] to regional [e.g., *Phadnis and Carmichael*, 2000] and box models [e.g., *Trentmann et al.*, 2005; *Mason et al.*, 2006], have also investigated this issue with most studies showing some degree of O_3 formation. This subject is treated in depth by *Jaffe and Wigder* [2012].

4. Summary

During the NCAR/NSF GV and NASA DC-8 research flights on 22 June 2012, the outflow from three convective storm cells near the Colorado-Nebraska border was studied at a time when the High Park fire had been burning for over a week. Aged smoke from the fire was sampled during the flight, as evidenced by enhancements in the BB tracers HCN and ACN. Acrolein was also elevated particularly in the NS outflow, indicating that the emissions sampled were only hours old. Acrolein proved to be a good fire tracer for fresh fire emissions, and this was validated by photochemical lifetime calculations using toluene to benzene ratios.

Box modeling predicts substantial downwind ozone production in the UT for both the fresh BB-impacted NS storm and more aged BB-impacted SS, whereas very little ozone production is predicted for transported air outside the outflow. The SS was predicted to produce more ozone over 2 days (14 ppbv) than the NS (11 ppbv) despite having lower VOC OH reactivity. Sensitivity tests showed that this was principally due to more NO_x being present in the SS outflow because of LNO_x. In fact, in the absence of LNO_x, the SS was predicted to produce only about 2 ppbv of ozone over 2 days, but with LNO_x a much higher ozone production efficiency leads to the predicted 14 ppbv ozone.

NEMRs were determined for the three BB tracers observed in the High Park fire. HCN and ACN were determined from both the DC-8 and GV measurements. They were found to be generally consistent with literature values although they are the first such measurements documented that are specific to the Front Range region. The NEMR for acrolein represents the first ambient measurement recorded and is generally consistent with published laboratory-based BB studies.

Acknowledgments

The data used in this paper are available from http://www-air.larc.nasa.gov/cgi-bin/ArcView/dc3-seac4rs and http://catalog.eol.ucar.edu/dc3_2012/index.html. The NCAR MM can be downloaded from the NCAR community data portal (http://cdp.ucar.edu/). The authors thank the crew and support team of the NSF/NCAR GV aircraft and Christine Wiedinmyer, Jeff Stith, and Shawn Honomichl for their helpful comments and discussion. The National Center for Atmospheric Research is sponsored by the National Science Foundation. Any opinions, findings, and conclusions or recommendations expressed in the publication are those of the authors and do not necessarily reflect the views of the National Science Foundation.

References

Aiken, A. C., et al. (2010), Mexico city aerosol analysis during MILAGRO using high resolution aerosol mass spectrometry at the urban supersite (T0)—Part 2: Analysis of the biomass burning contribution and the non-fossil carbon fraction, *Atmos. Chem. Phys.*, *10*(12), 5315–5341, doi:10.5194/acp-10-5315-2010.

Akagi, S. K., R. J. Yokelson, C. Wiedinmyer, M. J. Alvarado, J. S. Reid, T. Karl, J. D. Crounse, and P. O. Wennberg (2011), Emission factors for open and domestic biomass burning for use in atmospheric models, *Atmos. Chem. Phys.*, *11*(9), 4039–4072, doi:10.5194/acp-11-4039-2011.

Alvarado, M. J., et al. (2010), Nitrogen oxides and PAN in plumes from boreal fires during ARCTAS-B and their impact on ozone: An integrated analysis of aircraft and satellite observations, *Atmos. Chem. Phys.*, *10*(20), 9739–9760, doi:10.5194/acp-10-9739-2010.

Andreae, M. O., and P. Merlet (2001), Emission of trace gases and aerosols from biomass burning, *Global Biogeochem. Cycles*, *15*, 955–966, doi:10.1029/2000GB001382.
Apel, E. C., A. J. Hills, R. Lueb, S. Zindel, S. Eisele, and D. D. Riemer (2003), A fast-GC/MS system to measure C_2 to C_4 carbonyls and methanol aboard aircraft, *J. Geophys. Res.*, *108*(D20), 8794, doi:10.1029/2002JD003199.
Apel, E. C., et al. (2010), Chemical evolution of volatile organic compounds in the outflow of the Mexico City Metropolitan area, *Atmos. Chem. Phys.*, *10*, 2353–2375, doi:10.5194/acp-10-2353-2010.
Apel, E. C., et al. (2012), Impact of the deep convection of isoprene and other reactive trace species on radicals and ozone in the upper troposphere, *Atmos. Chem. Phys.*, *12*(2), 1135–1150, doi:10.5194/acp-12-1135-2012.
Apel, E. C., et al. (2013), Transport and chemical evolution of trace species following convective events during DC3, paper presented at 2013 Fall Meeting, AGU.
Brune, W. H., et al. (1998), Airborne in-situ OH and HO_2 observations in the cloud-free troposphere and lower stratosphere during SUCCESS, *Geophys. Res. Lett.*, *25*, 1701–1704, doi:10.1029/97GL03098.
Brunner, D., J. Staehelin, and D. Jeker (1998), Large-scale nitrogen oxide plumes in the tropopause region and implications for ozone, *Science*, *282*, 1305–1309.
Colman, J. J., A. L. Swanson, S. Meinardi, B. C. Sive, D. R. Blake, and F. S. Rowland (2001), Description of the analysis of a wide range of volatile organic compounds in whole air samples collected during PEM-TROPICS A and B, *Anal. Chem.*, *73*, 3723–3731, doi:10.1021/ac010027g.
Colomb, A., et al. (2006), Airborne measurements of trace organic species in the upper troposphere over Europe: The impact of deep convection, *Environ. Chem.*, *3*(4), 244–259, doi:10.1071/en06020.
Crawford, J. H., et al. (2000), Evolution and chemical consequences of lightning-produced NO_x observed in the North Atlantic upper troposphere, *J. Geophys. Res.*, *105*, 19,795–19,809, doi:10.1029/2000JD900183.
Crounse, J. D., et al. (2009), Biomass burning and urban air pollution over the Central Mexican Plateau, *Atmos. Chem. Phys.*, *9*, 4929–4944, doi:10.5194/acp-9-4929-2009.
de Gouw, J. A., C. Warneke, D. D. Parrish, J. S. Holloway, M. Trainer, and F. C. Fehsenfeld (2003), Emission sources and ocean uptake of acetonitrile (CH_3CN) in the atmosphere, *J. Geophys. Res.*, *108*(D11), 4329, doi:10.1029/2002JD002897.
de Gouw, J. A., et al. (2005), Budget of organic carbon in a polluted atmosphere: Results from the New England Air Quality Study in 2002, *J. Geophys. Res.*, *110*, D16305, doi:10.1029/2004JD005623.
de Gouw, J. A., et al. (2006), Volatile organic compounds composition of merged and aged forest fire plumes from Alaska and western Canada, *J. Geophys. Res.*, *111*, D10303, doi:10.1029/2005JD006175.
Dickerson, R. R., et al. (1987), Thunderstorms: An important mechanism in the transport of air pollutants, *Science*, *235*, 460–465.
Dye, J. E., et al. (2000), An overview of the Stratosphere-Troposphere Experiment: Radiation, Aerosols, and Ozone (STERAO)-Deep Convection experiment with results for the July 10, 1996 storm, *J. Geophys. Res.*, *105*, 10,023–10,045, doi:10.1029/1999JD901116.
Eisele, F. L., et al. (2003), Summary of measurement intercomparisons during TRACE-P, *J. Geophys. Res.*, *108*(D20), 8791, doi:10.1029/2002JD003167.
Forster, P. M. D., and K. P. Shine (1997), Radiative forcing and temperature trends from stratospheric ozone changes, *J. Geophys. Res.*, *102*, 10,841–10,855, doi:10.1029/96JD03510.
Fried, A., et al. (2008), Role of convection in redistributing formaldehyde to the upper troposphere over North America and the North Atlantic during the summer 2004 INTEX campaign, *J. Geophys. Res.*, *113*, D17306, doi:10.1029/2007JD009760.
Friedli, H. R., E. Atlas, V. R. Stroud, L. Giovanni, T. Campos, and L. F. Radke (2001), Volatile organic trace gases emitted from North American wildfires, *Global Biogeochem. Cycles*, *15*, 435–452, doi:10.1029/2000GB001328.
Fromm, M., J. Alfred, K. Hoppel, J. Hornstein, R. Bevilacqua, E. Shettle, R. Servranckx, Z. Q. Li, and B. Stocks (2000), Observations of boreal forest fire smoke in the stratosphere by POAM III, SAGE II, and lidar in 1998, *Geophys. Res. Lett.*, *27*, 1407–1410, doi:10.1029/1999GL011200.
Gelencsér, A., K. Siszler, and J. Hlavay (1997), Toluene−benzene concentration ratio as a tool for characterizing the distance from vehicular emission sources, *Environ. Sci. Technol.*, *31*, 2869–2872.
Gerbig, C., S. Schmitgen, D. Kley, A. Volz-Thomas, K. Dewey, and D. Haaks (1999), An improved fast-response vacuum-UV resonance fluorescence CO instrument, *J. Geophys. Res.*, *104*, 1699–1704, doi:10.1029/1998JD100031.
Gilman, J. B., B. M. Lerner, W. C. Kuster, and J. A. de Gouw (2013), Source signature of volatile organic compounds from oil and natural gas operations in Northeastern Colorado (vol 47, pg 1297, 2013), *Environ. Sci. Technol.*, *47*(17), 10,094, doi:10.1021/es4036978.
Guenther, A. B., and A. J. Hills (1998), Eddy covariance measurement of isoprene fluxes, *J. Geophys. Res.*, *103*, 13,145–13,152, doi:10.1029/97JD03283.
Hamm, S., and P. Warneck (1990), The interhemispheric distribution and the budget of acetonitrile in the troposphere, *J. Geophys. Res.*, *95*, 20,593–20,606, doi:10.1029/JD095iD12p20593.
Hornbrook, R. S., et al. (2011), Observations of non-methane organic compounds during ARCTAS—Part 1: Biomass burning emissions and plume enhancements, *Atmos. Chem. Phys.*, *11*, 11,103–11,130, doi:10.5194/acp-11-11103-2011.
Hudman, R. C., et al. (2007), Surface and lightning sources of nitrogen oxides over the United States: Magnitudes, chemical evolution, and outflow, *J. Geophys. Res.*, *112*, D12S05, doi:10.1029/2006JD007912.
Intergovernmental Panel on Climate Change (2013), *Climate Change 2013: The Physical Science Basis, the IPCC Fifth Assessment Report*, Geneva, Switzerland. [Available at https://www.ipcc.ch/report/ar5/wg1/.]
Jaffe, D. A., and N. L. Wigder (2012), Ozone production from wildfires: A critical review, *Atmos. Environ.*, *51*, 1–10, doi:10.1016/j.atmosenv.2011.11.063.
Jaffe, D. A., N. Wigder, N. Downey, G. Pfister, A. Boynard, and S. B. Reid (2013), Impact of wildfires on ozone exceptional events in the Western U.S., *Environ. Sci. Technol.*, *47*(19), 11,065–11,072, doi:10.1021/es402164f.
Johnson, R. H., R. S. Schumacher, J. H. Ruppert Jr., and D. T. Lindsey (2014), Meteorology of the Waldo Canyon fire, *Mon. Weather Rev.*, *142*, 3061–3080, doi:10.1175/MWR-D-13-00361.1.
Jost, H. J., et al. (2004), In-situ observations of mid-latitude forest fire plumes deep in the stratosphere, *Geophys. Res. Lett.*, *31*, L11101, doi:10.1029/2003GL019253.
Knighton, W. B., E. C. Fortner, A. J. Midey, A. A. Viggiano, S. C. Herndon, E. C. Wood, and C. E. Kolb (2009), HCN detection with a proton transfer reaction mass spectrometer, *Int. J. Mass Spectrom.*, *283*(1–3), 112–121, doi:10.1016/j.ijms.2009.02.013.
Konovalov, I. B., M. Beekmann, B. D'Anna, and C. George (2012), Significant light induced ozone loss on biomass burning aerosol: Evidence from chemistry-transport modeling based on new laboratory studies, *Geophys. Res. Lett.*, *39*, L17807, doi:10.1029/2012GL052432.
Kostenidou, E., C. Kaltsonoudis, M. Tsiflikiotou, E. Louvaris, L. M. Russell, and S. N. Pandis (2013), Burning of olive tree branches: A major organic aerosol source in the Mediterranean, *Atmos. Chem. Phys.*, *13*(17), 8797–8811, doi:10.5194/acp-13-8797-2013.
Lacis, A. A., D. J. Wuebbles, and J. A. Logan (1990), Radiative forcing of climate by changes in the vertical-distribution of ozone, *J. Geophys. Res.*, *95*, 9971–9981, doi:10.1029/JD095iD07p09971.

Lang, T. J., S. A. Rutledge, B. Dolan, P. Krehbiel, W. Rison, and D. T. Lindsey (2014), Lightning in wildfire smoke plumes observed in Colorado during summer 2012, *Mon. Weather Rev.*, *142*, 489–507.

Le Breton, M., et al. (2013), Airborne hydrogen cyanide measurements using a chemical ionisation mass spectrometer for the plume identification of biomass burning forest fires (Vol 13, Pg 9217, 2013), *Atmos. Chem. Phys.*, *13*(19), 9915.

Lewis, A. C., N. Carslaw, P. J. Marriott, R. M. Kinghorn, P. Morrison, A. L. Lee, K. D. Bartle, and M. J. Pilling (2000), A larger pool of ozone-forming carbon compounds in urban atmospheres, *Nature*, *405*, 778–781, doi:10.1038/35015540.

Li, Q., P. I. Palmer, H. C. Pumphrey, P. Bernath, and E. Mahieu (2009), What drives the observed variability of HCN in the troposphere and lower stratosphere?, *Atmos. Chem. Phys.*, *9*(21), 8531–8543, doi:10.5194/acp-9-8531-2009.

Li, Q. B., D. J. Jacob, I. Bey, R. M. Yantosca, Y. J. Zhao, Y. Kondo, and J. Notholt (2000), Atmospheric hydrogen cyanide (HCN): Biomass burning source, ocean sink?, *Geophys. Res. Lett.*, *27*, 357–360, doi:10.1029/1999GL010935.

Li, Q. B., D. J. Jacob, R. M. Yantosca, C. L. Heald, H. B. Singh, M. Koike, Y. J. Zhao, G. W. Sachse, and D. G. Streets (2003), A global three-dimensional model analysis of the atmospheric budgets of HCN and CH_3CN: Constraints from aircraft and ground measurements, *J. Geophys. Res.*, *108*(D21), 8827, doi:10.1029/2002JD003075.

Lipari, F., J. M. Dasch, and W. F. Scruggs (1984), Aldehyde emissions from wood-burning fireplaces, *Environ. Sci. Technol.*, *18*(5), 326–330, doi:10.1021/es00123a007.

Madronich, S. (2006), Chemical evolution of gaseous air pollutants down-wind of tropical megacities: Mexico City case study, *Atmos. Environ.*, *40*, 6012–6018.

Madronich, S., and S. Flocke (1999), The role of solar radiation in atmospheric chemistry, in *Handbook of Environmental Chemistry*, edited by P. Boule, pp. 1–26, Springer, Heidelberg, Germany.

Magneron, I., R. Thevenet, A. Mellouki, G. Le Bras, G. K. Moortgat, and K. Wirtz (2002), A study of the photolysis and OH-initiated oxidation of acrolein and trans-crotonaldehyde, *J. Phys. Chem. A*, *106*(11), 2526–2537, doi:10.1021/jp013413a.

Martin, R. V., et al. (2002), Interpretation of TOMS observations of tropical tropospheric ozone with a global model and in situ observations, *J. Geophys. Res.*, *107*(D18), 4351, doi:10.1029/2001JD001480.

Mason, S. A., J. Trentmann, T. Winterrath, R. J. Yokelson, T. J. Christian, L. J. Carlson, T. R. Warner, L. C. Wolfe, and M. O. Andreae (2006), Intercomparison of two box models of the chemical evolution in biomass-burning smoke plumes, *J. Atmos. Chem.*, *55*(3), 273–297, doi:10.1007/s10874-006-9039-5.

Murray, L. T., D. J. Jacob, J. A. Logan, R. C. Hudman, and W. J. Koshak (2012), Optimized regional and interannual variability of lightning in a global chemical transport model constrained by LIS/OTD satellite data, *J. Geophys. Res.*, *117*, D20307, doi:10.1029/2012JD017934.

Nassar, R., J. A. Logan, I. A. Megretskaia, L. T. Murray, L. Zhang, and D. B. A. Jones (2009), Analysis of tropical tropospheric ozone, carbon monoxide, and water vapor during the 2006 El Niño using TES observations and the GEOS-Chem model, *J. Geophys. Res.*, *114*, D17304, doi:10.1029/2009JD011760.

Pétron, G., et al. (2012), Hydrocarbon emissions characterization in the Colorado Front Range: A pilot study, *J. Geophys. Res.*, *117*, D04304, doi:10.1029/2011JD016360.

Pétron, G., et al. (2014), A new look at methane and nonmethane hydrocarbon emissions from oil and natural gas operations in the Colorado Denver-Julesburg Basin, *J. Geophys. Res. Atmos.*, *119*, 6836–6852, doi:10.1002/2013JD021272.

Pfister, G. G., et al. (2006), Ozone production from the 2004 North American boreal fires, *J. Geophys. Res.*, *111*, D24S07, doi:10.1029/2006JD007695.

Pfister, G. G., C. Wiedinmyer, and L. K. Emmons (2008), Impacts of the fall 2007 California wildfires on surface ozone: Integrating local observations with global model simulations, *Geophys. Res. Lett.*, *35*, L19814, doi:10.1029/2008GL034747.

Phadnis, M. J., and G. R. Carmichael (2000), Forest fire in the Boreal Region of China and its impact on the photochemical oxidant cycle of East Asia, *Atmos. Environ.*, *34*(3), 483–498, doi:10.1016/s1352-2310(99)00249-6.

Pickering, K. E., A. M. Thompson, R. R. Dickerson, W. T. Luke, D. P. McNamara, J. P. Greenberg, and P. R. Zimmerman (1990), Model calculations of tropospheric ozone production potential following observed convective events, *J. Geophys. Res.*, *95*, 14,049–14,062, doi:10.1029/JD095iD09p14049.

Pickering, K. E., A. M. Thompson, J. R. Scala, W. K. Tao, R. R. Dickerson, and J. Simpson (1992), Free tropospheric ozone production following entrainment of urban plumes into deep convection, *J. Geophys. Res.*, *97*, 17,985–18,000, doi:10.1029/92JD01716.

Pollack, I. B., et al. (2012), Airborne and ground-based observations of a weekend effect in ozone, precursors, and oxidation products in the California South Coast Air Basin, *J. Geophys. Res.*, *117*, D00V05, doi:10.1029/2011JD016772.

Randel, W. J., M. Park, L. Emmons, D. Kinnison, P. Bernath, K. A. Walker, C. Boone, and H. Pumphrey (2010), Asian monsoon transport of pollution to the stratosphere, *Science*, *328*(5978), 611–613, doi:10.1126/science.1182274.

Ridley, B. A., and F. E. Grahek (1990), A small, low flow, high-sensitivity reaction vessel for NO chemiluminescence detectors, *J. Atmos. Oceanic Technol.*, *7*(2), 307–311, doi:10.1175/1520-0426(1990)007<0307:aslfhs>2.0.co;2.

Ridley, B. A., F. E. Grahek, and J. G. Walega (1992), A small, high-sensitivity, medium-response ozone detector suitable for measurements from light aircraft, *J. Atmos. Oceanic Technol.*, *9*(2), 142–148, doi:10.1175/1520-0426(1992)009<0142:ashsmr>2.0.co;2.

Ridley, B. A., J. G. Walega, J. E. Dye, and F. E. Grahek (1994), Distributions of NO, NO_x, NO_y, and O_3 to 12 km altitude during the summer monsoon season over New Mexico, *J. Geophys. Res.*, *99*, 25,519–25,534, doi:10.1029/94JD02210.

Ridley, B. A., et al. (2004), Florida thunderstorms: A faucet of reactive nitrogen to the upper troposphere, *J. Geophys. Res.*, *109*, D17305, doi:10.1029/2004JD004769.

Rison, W., R. J. Thomas, P. R. Krehbiel, T. Hamlin, and J. Harlin (1999), A GPS-based three-dimensional lightning mapping system: Initial observations in central New Mexico, *Geophys. Res. Lett.*, *26*, 3573–3576, doi:10.1029/1999GL010856.

Ryerson, T. B., E. J. Williams, and F. C. Fehsenfeld (2000), An efficient photolysis system for fast-response NO_2 measurements, *J. Geophys. Res.*, *105*, 26,447–26,461, doi:10.1029/2000JD900389.

Sander, R. (1999), Modeling atmospheric chemistry: Interactions between gas-phase species and liquid cloud/aerosol particles, *Surv. Geophys.*, *20*(1), 1–31, doi:10.1023/a:1006501706704.

Shim, C., Y. Wang, H. B. Singh, D. R. Blake, and A. B. Guenther (2007), Source characteristics of oxygenated volatile organic compounds and hydrogen cyanide, *J. Geophys. Res.*, *112*, D10305, doi:10.1029/2006JD007543.

Simpson, I. J., et al. (2011), Boreal forest fire emissions in fresh Canadian smoke plumes: C-1-C-10 volatile organic compounds (VOCs), CO_2, CO, NO_2, NO, HCN and CH_3CN, *Atmos. Chem. Phys.*, *11*, 6445–6463, doi:10.5194/acp-11-6445-2011.

Singh, H. B., et al. (2003), In situ measurements of HCN and CH_3CN over the Pacific Ocean: Sources, sinks, and budgets, *J. Geophys. Res.*, *108*(D20), 8795, doi:10.1029/2002JD003006.

Singh, H. B., et al. (2007), Reactive nitrogen distribution and partitioning in the North American troposphere and lowermost stratosphere, *J. Geophys. Res.*, *112*, D12S04, doi:10.1029/2006JD007664.

Singh, H. B., C. Cai, A. Kaduwela, A. Weinheimer, and A. Wisthaler (2012), Interactions of fire emissions and urban pollution over California: Ozone formation and air quality simulations, *Atmos. Environ.*, *56*, 45–51, doi:10.1016/j.atmosenv.2012.03.046.

Slusher, D. L., L. G. Huey, D. J. Tanner, F. M. Flocke, and J. M. Roberts (2004), A thermal dissociation-chemical ionization mass spectrometry (TD-CIMS) technique for the simultaneous measurement of peroxyacyl nitrates and dinitrogen pentoxide, *J. Geophys. Res.*, *109*, D19315, doi:10.1029/2004JD004670.

Snow, J. A., B. G. Heikes, H. W. Shen, D. W. O'Sullivan, A. Fried, and J. Walega (2007), Hydrogen peroxide, methyl hydroperoxide, and formaldehyde over North America and the North Atlantic, *J. Geophys. Res.*, *112*, D12S07, doi:10.1029/2006JD007746.

Spada, N., E. Fujii, and T. M. Cahill (2008), Diurnal cycles of acrolein and other small aldehydes in regions impacted by vehicle emissions, *Environ. Sci. Technol.*, *42*(19), 7084–7090, doi:10.1021/es801656e.

Sprengnether, M., K. L. Demerjian, N. M. Donahue, and J. G. Anderson (2002), Product analysis of the OH oxidation of isoprene and 1,3-butadiene in the presence of NO, *J. Geophys. Res.*, *107*(D15), 4268, doi:10.1029/2001JD000716.

Stickler, A., H. Fischer, J. Williams, M. de Reus, R. Sander, M. G. Lawrence, J. N. Crowley, and J. Lelieveld (2006), Influence of summertime deep convection on formaldehyde in the middle and upper troposphere over Europe, *J. Geophys. Res.*, *111*, D14308, doi:10.1029/2005JD007001.

Trentmann, J., R. J. Yokelson, P. V. Hobbs, T. Winterrath, T. J. Christian, M. O. Andreae, and S. A. Mason (2005), An analysis of the chemical processes in the smoke plume from a savanna fire, *J. Geophys. Res.*, *110*, D12301, doi:10.1029/2004JD005628.

Warneke, C., et al. (2009), Biomass burning in Siberia and Kazakhstan as an important source for haze over the Alaskan Arctic in April 2008, *Geophys. Res. Lett.*, *36*, L02813, doi:10.1029/2008GL036194.

Warneke, C., J. M. Roberts, P. Veres, J. Gilman, W. C. Kuster, I. Burling, R. Yokelson, and J. A. de Gouwa (2011), VOC identification and inter-comparison from laboratory biomass burning using PTR-MS and PIT-MS, *Int. J. Mass Spectrom.*, *303*(1), 6–14, doi:10.1016/j.ijms.2010.12.002.

Weibring, P., D. Richter, J. G. Walega, L. Rippe, and A. Fried (2010), Difference frequency generation spectrometer for simultaneous multispecies detection, *Opt. Express*, *18*(26), 27,670–27,681.

Yokelson, R. J., T. Karl, P. Artaxo, D. R. Blake, T. J. Christian, D. W. T. Griffith, A. Guenther, and W. M. Hao (2007a), The tropical forest and fire emissions experiment: Overview and airborne fire emission factor measurements, *Atmos. Chem. Phys.*, *7*(19), 5175–5196.

Yokelson, R. J., et al. (2007b), Emissions from forest fires near Mexico City, *Atmos. Chem. Phys.*, *7*(21), 5569–5584.

Yokelson, R. J., et al. (2009), Emissions from biomass burning in the Yucatan, *Atmos. Chem. Phys.*, *9*, 5785–5812, doi:10.5194/acp-9-5785-2009.

Yokelson, R. J., et al. (2013), Coupling field and laboratory measurements to estimate the emission factors of identified and unidentified trace gases for prescribed fires, *Atmos. Chem. Phys.*, *13*, 89–116, doi:10.5194/acp-13-89-2013.